Resistivity and low-frequency noise characteristics of epoxy-carbon composites

Sandra Pralgauskaitė, Jonas Matukas, Marina Tretjak, Jan Macutkevic, Juras Banys, Algirdas Selskis, Antonino Cataldo, Federico Micciulla, Stefano Bellucci, Vanessa Fierro, et al.

Resistivity and low-frequency noise characteristics of epoxy-carbon composites

Sandra Pralgauskaitė[1], Jonas Matukas[1], Marina Tretjak[1], Jan Macutkevic[1], Juras Banys[1], Algirdas Selskis[2], Antonino Cataldo[3], Federico Micciulla[3], Stefano Bellucci[3], Vanessa Fierro[4], Alain Celzard[4]

[1]Radiophysics Department, Vilnius University, Sauletekio 9, LT10022, Vilnius, Lithuania

[2]Center for Physical Science and Technology, Vilnius University, Sauletekio 9, LT10022, Vilnius, Lithuania

[3]Frascati National Laboratory, National Institute of Nuclear Physics, Via E. Fermi 40, 00044 Frascati, Italy

[4]IJL – UMR CNRS 7198, ENSTIB, 27 rue Philippe Séguin, CS 60036, 88026 Épinal Cedex, France

jan.macutkevic@gmail.com

Noise and electrical transport properties of composites based on epoxy resin filled with various carbon inclusions (single-walled carbon nanotubes, high surface area carbon black and exfoliated graphite) were investigated in depth. The temperature dependence of resistivity shows that Mott's hopping and tunneling between conductive carbon particles dominate the charge carrier transport at low temperature, whereas a positive temperature coefficient (PTC) effect occurs at higher temperature. Low-frequency noise spectra of investigated materials comprise $1/f^{\alpha}$ type components. The noise level

is the highest for composites close to the percolation threshold. The percolation threshold value of the system also strongly impacts both the temperature dependence of noise level and the resistivity. Close to the percolation threshold, the noise level increases due to the carrier tunneling throughout the polymer matrix and decreases due to the rapid expansion of the polymer matrix. In contrast, the latter has almost no influence on the noise level far above the percolation threshold, and the small kink in the temperature dependence of the noise level indicates a crossover between tunneling and thermally activated electron transport mechanisms.

Introduction

It is well known that carbon nanotubes (CNTs) are potential candidates for being used in various nanostructures and nano-devices such as nano-sized transistors, field effect transistors [1], nanoscale terahertz devices, micro-scale inductors [2], sensors [3, 4], etc. Those versatile nanoscale electronics applications are possible due to a unique combination of structural and physical properties presented by CNTs, e.g. one-dimensional tubular structure, fast response and low working temperature, strength and durability, flame resistance, vapor adsorption, UV absorption, etc.

One more advantage of carbon nanotubes is their presumed immunity to excess electrical noise that in general tends to increase dramatically as the dimensions of the devices decrease. Carbon nanotubes behaving as covalently bonded metallic wires might be less susceptible to such fluctuations. The strong carbon-carbon bonds which form the nanotube should indeed not be prone to electro-migration or defect propagation, which are two of the most important noise mechanisms in standard metal films and wires [5, 6].

Electrical conductivity studies in disordered solids are a topic of considerable interest [7-9]. Both metallic and non-metallic behaviors can be observed, as well as abrupt jumps of conductivity when the temperature is varied [10]. The results suggest that all these systems can be regarded as random resistive networks of tunnel junctions formed by adjacent carbon nanotubes [11]. Electrical and electromagnetic properties of carbon nanotubes composites also greatly depend on nanotubes orientation and distribution in the polymer matrix [12-14].

It is also well known that noise characteristics are extremely sensitive to the physical processes taking place in various materials and structures, and therefore can provide valuable information on charge carriers transport and conduction mechanisms [15-18]. Nevertheless, investigations of noise in CNT-based materials are rare [11, 19-21], while electrical and magnetic properties of the same materials are thoroughly investigated in the literature. It has been shown [20] that the measured magnitude of $1/f$ noise in individual isolated carbon nanotubes, thin films of interconnected nanotubes, and bulk nanotube mats greatly exceeds the one commonly observed in more conventional conductors, i.e., metal films, carbon resistors or even carbon fibers having comparable resistances. The large noise level suggests the importance of surface mechanisms: any adsorbate or intercalant affecting CNTs electronically might also be expected to play a role in the generation of $1/f$ noise, because every atom that constitutes CNTs is a surface atom. In other words, the external surface area of CNTs is quite high [1, 20]. On the other hand, the contribution to $1/f$ noise, not only by nanotubes themselves but by the material in which they are embedded, should be taken into account [19, 21-23]. It has also been shown that, above the percolation threshold (i.e., the critical concentration of conductive filler at which a composite undergoes an insulator – conductor transition), the resistivity of the composites can increase with the temperature, and this can be explained by the thermal expansion of the polymer matrix which results in the breakdown of the CNT network [23]. This phenomenon is well-known in polymer

(nano)composites and is referred to as a positive temperature coefficient (PTC) effect. Altogether, 1/*f* noise level in CNT-based composites depends strongly on device dimensions, nanotube degree of alignment, and film resistivity [1, 3, 20, 23].

In such a context, the aim of the present work was to clear up the physical processes occurring in epoxy-carbon composites and to determine the charge carrier transport mechanisms by low-frequency noise measurements.

Materials

Different carbon materials dispersed in epoxy resin were investigated: single-walled carbon nanotubes (SWCNTs), high surface-area carbon black (CBH), and exfoliated graphite (EG). The electromagnetic and mechanical properties of the corresponding composites were reported elsewhere [24, 25].

Commercially available SWCNTs from Heji were used for CNT/resin composite fabrication. The synthesis method of SWCNTs was CVD. The SWCNT data are the following: diameter 1–2 nm, mostly in bundles of 8–20 nm; length 10–20 μm; apparent density 0.3 g/cm^3 at 25°C; 90 % purity. A representative Transmission Electron Microscopy (TEM) image of SWCNT is given in Fig. 1a.

Commercially available ENSACO 350G conductive carbon black of High surface area (CBH: BET surface area = 770 m^2/g; oil absorption = 320 mL/100g) was kindly supplied by Timcal Ltd. (Bodio, Switzerland). Such material is widely used as black pigment, UV stabilizer, and rubber reinforcement, and allows the retention of a carbon network at low to very low filler content. Its high void volume originates from the interstices between the carbon black particles, due to their complex arrangement, and from the porosity. A typical TEM image of CBH is presented in Fig. 2b, and shows

that the aggregates can be as large as 500 nm and are based on spherical particles of diameter close to 10 nm, as expected for this kind of material.

Exfoliated graphite was purchased from Mersen (France). It is a material of extremely low packing density, around 0.003 g cm^{-3}, based on highly porous, accordion-like particles [26]. Typically, the diameter of the EG particles is in the range 0.3-0.5 mm, and their aspect ratio is around 20. A typical Scanning Electron Microscopy (SEM) image of EG is presented in Fig. 1c.

EPIKOTE™ Resin 828 was used as composite matrix. It is a medium viscosity liquid epoxy produced from bisphenol A resin and epichlorhydrin. It contains no diluent. EPIKOTE 828 provides good pigment wetting and good resistance to filler settling and high mechanical and chemical resistance in the cured state.

The fabrication of SWCNTs-, CBH- and EG-based composites was carried out along with the same method. A series of composite samples made of Epikote 828 epoxy resin, a curing agent called A1 (a modified tetraethylenepentamine) and 0.25, 0.5, 1.0, 1.5 and 2.0 wt.% of carbon filler were fabricated as follows: the resin was degassed under vacuum (1–3 mbar) for 12–14 h, then it was put into an oven at 338 K. In the meantime, the carbon filler was dispersed in propanol through ultrasonic bath for 1.5 h. Afterwards the solution of alcohol and carbon filler was mixed with the resin. The obtained mixture was inserted inside the oven at 403–423 K for the evaporation of alcohol. The mix was then poured into 1 cm × 1 cm × 7 cm molds, and left as such for 20 h for the curing process at room temperature and then for 4 h in an oven at 353 K. When the process was completed, the samples were removed from the molds. The uniformity of the distribution of carbon fillers in the polymer samples was studied by scanning electron microscopy, using a Helios NanoLab 650 microscope and examioning the samples at many places; all fabricated composites demonstrated good homogeneity, carbon inclusions being reasonably well dispersed (see, Fig. 2). The concentration of fillers in all

composites was 2 wt. %, which is above the percolation threshold (1.5, 0.25, and close to 0.5 wt.% in EG-, SWCNT-, and CBH-based composites, respectively [25]). Investigated samples were 3 mm-thick (except EG sample: 2 mm), and had areas of 2.57, 21 and 12 mm^2 for EG-, SWCNT-, and CBH-based composites, respectively.

Measurement technique

The low-frequency noise characteristics (current noise spectral density) were measured under constant voltage operation in a frequency range from 10 Hz to 20 kHz at temperatures ranging from 73 K to 380 K. The measured noise signal was processed by a low-noise amplifier, a filter system, and an analogue digital converter (National Instrument^{TM} PCI 6115 board) [25]. The noise measurements were performed in a specially shielded room (Faraday cage) in order to avoid interferences from electrical network and communication systems. The measuring scheme is presented in Fig. 3. The load resistance, R_{load}, was at least 30 times larger than the resistance of the investigated samples.

The current noise spectral density, S_I, was calculated using the standard Cooley–Tukey Fast Fourier Transform algorithm and evaluated by comparison with the thermal noise of the standard resistor (described by Nyquist's theorem), which was at room temperature, and used also as the load resistor [28]:

$$S_I = \frac{\overline{U^2}-\overline{U_S^2}}{\overline{U_{\mathrm{st}}^2}-\overline{U_S^2}}\frac{4kT_0}{R_{\mathrm{load}}}; \qquad (1)$$

where $\overline{U^2}$, $\overline{U_S^2}$ and $\overline{U_{\mathrm{st}}^2}$ are sample, measuring system, and standard resistor thermal noise variances in the narrow frequency band Δf; T_0 is the absolute temperature of the standard resistor, and k is the Boltzmann constant.

Results and discussion

Resistivity dependence on voltage and temperature

The resistivity values of the investigated materials were significantly different, depending on the type of carbon inclusions. Those based on EG were only a few tens of Ω·m, CBH – few kΩ·m, whereas those based on SWCNTs were a few hundreds of kΩ·m. In Fig. 4a, the static characteristics of the investigated materials are presented at room temperature. Up to a voltage of 1 V (approximately 3.3 V/cm for SWCNT composites and 5 V/cm for EG composites), the resistivity is constant and therefore the current-voltage characteristic is linear. Above 1 V, the differential resistance of the materials changes and the current-voltage characteristics becomes super-linear. As expected for materials with conductive fillers, and as carbon nanoparticles can indeed be roughly treated as having a metallic conductance, the resistivity of the investigated materials is Ohmic at low electric field, but starts to decrease above a critical value. Charge carrier transport mechanisms that can be usually found in such materials are tunneling, transport through defect centers, and hopping [29]. Carbon particles' dimensions and the distance between them determine which transport mechanisms dominate in one given material. Also, for electrical transport, the orientation of carbon particles and the properties of the electrical contact between particles are very important [30-31].

At low temperatures (below 188 K in EG- and CBH-based samples, below 292 K in SWCNT-based sample), the resistivity decreases when the temperature increases (Fig. 4b). At these temperatures, the resistivity can be well approximated by [32]:

$$\lg R \sim (T_{02}/T)^{1/3}. \quad (2)$$

Such behavior is typical of two-dimensional hopping [32]. The values of T_0 are 324 K for SWCNT composites, 200 K for CBH composites and 2 K for EG composites. Moreover, in the same

temperature range, the resistivity can be well described by the fluctuation-induced tunneling model [33] (see Fig. 4c):

$$\rho = \rho_0 \exp\left(\frac{T_1}{T+T_0}\right); \quad (3)$$

where T is the temperature, T_0 is the characteristic temperature below which the dc conductivity reduces to temperature-independent tunneling, and T_1 reflects the energy required to move an electron across the insulating gap between conductive aggregates. The parameters obtained from the fit of the tunneling model (Eq. 3) to the experimental data are summarized in Table 1. Therefore, the carrier transport occurs at low temperature due to electrons hopping inside carbon cluster and tunneling between clusters. It is observed that the temperature of the minimum resistivity is lower for materials with EG and CBH fillers compared to the SWCNT-based samples. The higher value of the temperature of the minimum resistivity is related to the lower percolation threshold of SWCNT composites. The resistivity of the latter follows a simple Arrhenius law in the temperature range 145 - 292 K (see Fig. 4c), indicating that the conduction mechanism based on thermal activation over the potential barrier is predominant. Indeed, the conductivity based on thermal activation over the potential barrier can be described by equation [11]:

$$\rho = \rho_0 \exp\left(\frac{T_c T_1}{T(T_c+T_0)}(1-\varepsilon_A)^2\right) = \rho_0 \exp\left(\frac{\Delta E}{T}\right), \quad (4)$$

where T_c is the crossover temperature above which the fluctuation-induced tunneling and thermal activation contributions are indistinguishable, ε_A is the dimensionless applied electric field, and $\Delta E = T_c T_1/(T_c+T_0)$. The value of ΔE parameter in the temperature range 145 –292 K is 9.5 meV, which is in good agreement with T_c = 145 K and with the values of T_1 and T_0 obtained from the fitting at low temperatures.

The minimum in the temperature dependence of the resistivity is close to the polymer glass transition temperature. The values of the temperature corresponding to those minima of resistivity are

given in Table 1. Above these temperatures, the resistivity of composites increases due to the rapid expansion of the polymer matrix, thereby leading to the increase of the distance between conductive nanoparticles clusters at the micro scale and decreasing the electron tunneling current [34].

Noise measurement results

The low-frequency noise spectra coincide with $1/f^{\alpha}$ components with different α values (Fig. 5). $1/f^{\alpha}$ type fluctuations indicate that conduction mechanisms such as Mott's hopping between carbon nanoparticles and controlled by charge carrier capture in localized states between them are present.

$1/f^{\alpha}$ type noise level depends on investigated materials: for EG-based sample, $1/f^{\alpha}$ type fluctuations are the most intense, while for CBH- and SWCNT-based samples, $1/f^{\alpha}$ type noise is 2-3 orders of magnitude lower at the same current (Fig. 5). Larger $1/f^{\alpha}$ type noise intensity can be related to larger surface area presented by the carbon particles since the combination of many carrier capture and release processes through surface states leads to $1/f^{\alpha}$ fluctuations. Moreover, according to the percolation theory, the voltage spectral density close to the percolation threshold decreases with filler concentration according to the power law [35, 36]:

$$S_U/U^2 \approx (p - p_c)^{-k}; \quad (5)$$

and the following similar relation is valid for resistivity:

$$\rho \approx (p - p_c)^{-t} \quad (6)$$

where k and t are the critical exponents. Thus, the composites with the lowest percolation threshold, i.e., those with SWCNT inclusions, present the lowest noise level. Moreover, according to Eqs. (5) and (6), it should be expected that close to the percolation threshold:

$$S_U/U^2 \approx \rho^{k/t} \quad (7)$$

where k/t can range from 0.87 to 3.2 for various random-void models [36]. However, Eq. (7) cannot explain the relation between the noise level and the resistivity in a broad temperature range because both k and t are temperature-dependent [37].

The noise spectral density characteristics at 86.13 Hz are presented in Fig. 5b, where $1/f^{\alpha}$ type noise dominates. It is found that the spectral density of current fluctuation is approximately proportional to the squared flowing current. Such proportionality of the current spectral density is characteristic for resistance fluctuations.

The temperature noise characteristics are presented in Fig. 6. All investigated materials have a maximum of current noise spectral density slightly below room temperature. The maximum is more significant at low frequencies, which indicates that it is related to $1/f^{\alpha}$ type noise. For composites with CBH and EG inclusions, the temperature at which the current noise spectral density passes through a maximum is substantially higher than that corresponding to the minimum of resistivity (see Fig. 7).

Just for the conductivity, the noise level decreases with temperature due to the rapid expansion of the polymer and to the induced increase of tunneling distances for charge carriers. However, if we assume some energy distribution of carriers, even the tunneling of a low amount of carriers with relatively high energy can contribute significantly to the noise. Therefore, the noise level increases with temperature until the distance between the carbon clusters becomes too high, even for high-energy carriers. This can explain that the temperature corresponding to the maximum of noise level is higher than the temperature of the minimum of resistivity.

Above room temperature, the noise level of composites with EG inclusions increases with temperature. Epoxy resin has negligibly low dc conductivity below 370 K [23], but the carrier density fluctuation in such insulator can somewhat appear at lower temperatures. Therefore, electron tunneling from the carbon clusters through the polymer matrix can impact the carrier's number in a random way

and thereby increase the noise level. This effect is observed only for EG-based composites, which are the closest to their percolation threshold. Therefore, EG-based materials are expected to have the lowest number of carriers, and this number can be mostly affected by electron tunneling throughout the matrix.

Some small kink is observed in the temperature dependence of the noise level for SWCNT-based composites close to 135 K (see Fig. 6). This temperature is very close to the temperature of a crossover between tunneling and thermal activation conductivity processes. The maximum of noise for SWCNT composites is close to 276 K, which is close to the resistivity minimum temperature (292 K).

The type of noise spectrum does not really change with temperature and remains $1/f^{\alpha}$. One exception was observed in the SWCNT-based material noise characteristics: some noise peaks are indeed observed at low frequencies at particular temperatures: 111 K and 135 K. The noise spectrum at those peaks is proportional to $1/f^2$. This indicates that the sample contains discrete, localized, centers of charge carriers that lead to enhanced charge carriers capture and release processes at particular temperatures, and to Lorentzian-type noise spectrum.

The noise level is presented versus the resistivity in Fig. 7 for all investigated composites. At low temperatures (for example for EG-based composites below 237 K), the decrease of the noise level is clearly observed and is consistent with the two-level tunneling system fluctuators model [38]:

$$S_U = \frac{AT}{R^2}. \quad (8)$$

At higher temperatures, composites with different inclusions demonstrate such particular behavior. For composites with SWCNT inclusions, the noise level decreases when the resistivity increases despite the fact that the conductivity follows the thermal activation law above 145 K. At the highest temperatures (above 230 K), the noise level is independent from the resistivity. The same almost applies to CBH-based composites at higher temperatures, as the classical dependence (Eq. 7) is

observed only in a narrow temperature range: k/t = 10.4 in 197-253 K. For EG-based composites, k/t = 1.3 in the temperature range 308-352 K. The latter k/t value is close to the value theoretically predicted in 2D inverted random-void model (k/t = 0.87).

Conclusions

Noise and electrical transport properties of carbon particles / epoxy resin composites were studied. The temperature dependence of the resistivity showed that, at low temperature, Mott's hopping and tunneling between conductive carbon particles dominated the transport of charge carriers whereas a positive temperature coefficient (PTC) effect occurred at higher temperature.

Low-frequency noise spectra of investigated materials comprised $1/f^{\alpha}$ type components. $1/f^{\alpha}$ fluctuations originated from Mott's hopping and combination of charge carriers capture and release processes. The noise level was the highest for the composites close to their percolation threshold. The percolation threshold value in the system strongly impacted the temperature dependence of the noise level and the resistivity. Close to the percolation threshold, the noise level increased due to tunneling throughout the polymer matrix and decreased due to the rapid expansion of the latter. In contrast, far above the percolation threshold, the matrix expansion had a very weak influence on the noise level, and the kink in the temperature dependence of noise level indicated a crossover between two electron transport mechanisms: tunneling and thermal activation. At higher temperatures, noise due electron tunneling into polymer matrix became also important.

References

1. T. Kawaharaa, S. Yamaguchia, Y. Ohnob, K. Maehashib, K. Matsumotob, S. Mizutanic, K. Itakad, Applied Surface Science **267**, 101 (2013).

2. B.S. Sreeja, Microelectronics Journal **45**, 196 (2014).

3. T. Li, X. Liu, Ch. Dong, L. Yin, Microelectronic Engineering **119**, 155 (2014).

4. B. Arash, Q. Wang, Scientific reports **3**, 1782 (2013).

5. P. Dutta, P. M. Horn, Rev. of Modern Phys. **53**, 497 (1981).

6. J. W. Eberhard, P. M. Horn, Phys. Rev. B **18**, 6681 (1978).

7. Ch. Li, E. T. Thostenson, T.-W. Chou, Appl. Phys. Lett. **91**, 223114 (2007).

8. *Carbon Nanotubes – Properties and Applications*, ed. by M. J. O'Connell (Taylor & Francis, LLC, Boca Raton, USA, 2006).

9. M. Sahimi, *Applications of Percolation Theory* (Taylor & Francis, LLC, Bristol, PA, 1994)

10. T. W. Ebbesen, H. J. Lezec, H. Hiura, J. W. Bennett, H. F. Ghaemi, and T. Thio, Nature **382**, 54 (1996).

11. C. Barone, G. Landi, C. Mauro, H. C. Neitzert, and S. Pagano, Appl. Phys. Lett. **107**, 143106, 2015.

12. M. Arjmand, M. Mahmoodi, G. A. Gelves, S. Park, U. Sundararaj, Carbon **49**, 3430 (2011).

13. A. K. Ghavidel, T. Azdast, M. Shabgard, A. Navidfar, and S. Sadighikia, J. Appl. Polym. Sci. **132**, 42671 (2015).

14. M. TabkhPaz, M. Mahmoodi, M. Arjmand, U. Sundararaj, J. Chu, S. S. Park, Macromolecular Materials and Engineering **300**, 482 (2015).

15. V. Palenskis, J. Matukas, J. Vyšniauskas, S. Pralgauskaitė, H. Shtrikman, D. Seliuta, I. Kašalynas, G. Valušis, Fluctuation and Noise Lett. **12**, 1350014 (2013).

16. V. Palenskis, J. Matukas, S. Pralgauskaitė, D. Seliuta, I. Kašalynas, L. Subačius, G. Valušis, S. P. Khanna, and E. H. Linfield, J. Appl. Phys. **113**, 083707 (2013).

17. S. Pralgauskaitė, V. Palenskis, J. Matukas, B. Šaulys, V. Kornijčuk, V. Verdingovas, Solide-State Electronis **79**, 104 (2013).

18. B.K. Jones, IEEE Trans. Electron Dev. **41** 2188 (1994).

19. A. Behnam, G. Bosman, and A. Ural, Phys. Rev. B **78**, 085431 (2008).

20. P. G. Collins, M. S. Fuhrer, A. Zettl, Appl. Phys. Lett. **76**, 894 (2000).

21. C. Barone, S. Pagano, and H. C. Neitzert, Appl. Phys. Lett. **97**, 152107 (2010).

22. F. N. Hooge, Physica B **83**, 14 (1976).

23. J. Macutkevic, P. P. Kuzhir, A. G. Paddubskaya, J. Banys, S. A. Maksimenko, E. Stefanutti, F. Micciulla, S. Bellucci, J. Nanophotonics **7**, 073593 (2013).

24. S. Bellucci,F. Micciulla, V. M. Levin, Yu. S. Petronyuk, L.A. Chernozatonskii, PP. Kuzhnir, A. G. Paddubskaya, J. Macutkevic, M. A. Pletnev, V. Fierro, A. Celzard, AIP Adv. 5, 067137 2015.

25. P. Kuzhir, A. Paddubskaya, A. Plyushch, N. Volynets, S. Maksimenko, J. Macutkevic, I. Kranauskaite, J. Banys, E. Ivanov, R. Kotsilkova, A. Celzard, V. Fierro, J. Zicans, T. Ivanova, R. Merijs Meri, I. Bochkov, A. Cataldo, F. Micciulla, S. Bellucci, Ph. Lambin, J. Appl. Phys. **114**, 164304 (2013).

26. A. Celzard, J.F. Marêché, G. Furdin, Prog. Mater. Sci. **50**, 93 (2005).

27. J. Banys, T. Ramoška, J. Matukas, S. Pralgauskaitė, F. M. M. Alawneh, V. V. Shvartsman, D. C. Lupascu , Ferroelectrics **417**, 25 (2011).

28. A. van der Ziel, *Noise in measurements* (John Wiley & Sons Inc., 1976).

29. D. van der Putten, S. T. Moonen, H. B. Brom, J. C. M. Brookken-Zijp and M. A. J. Michels, Phys. Rev. Lett. **69**, 494 (1992).

30. M. Mahmoodi, Ph. D. thesis, University of Calgary, 2013.

31. M. Arjmand, Ph. D. thesis, University of Calgary, 2014.

32. N. F. Mott, J. Non-Cryst Solids **8-10**, 1 (1972).

33. P. Sheng, Phys. Rev. B **21**, 2180 (1980).

34. Z. Ounaies, C. Park, K. E. Wise, E. J. Siochi, and J. S. Harrison, Composites Sci. and Technology **63**, 1637 (2003).

35. A. M. S. Tremblay, S. Feng, P. Breton, Phys. Rev. B **33**, 2077 (1986).

36. R. Rammal, C. Tannous, P. Breton, A. M. S. Tremblay, Phys. Rev. Lett. **54**, 1718 (1985).

37. H. M. Kim, M. S. Choi, J. Joo, S. J. Cho, H. S. Yoon, Phys. Rev. B 74, 054202 (2006).

38. S. Kogan, Electronic noise and fluctuations in solids (Cambridge university press, Cambridge, 1996).

Figures

Fig. 1. Microscopy images of carbon particles used for composite preparation: TEM images of (a) SWCNT and (c) CBH; (b) SEM image of EG.

Fig. 2. SEM images of composites based on: (a) CBH; (b) EG, and (c) SWCNT fillers.

Fig. 3. Scheme of the noise measuring system.

Fig. 4. Resistivity dependence: (a) on voltage at 290 K; and (b) on temperature (sample voltage was 150 mV for EG, 4.6 V for CBH, and 69 V for SWCNT); (c) Fit of Eq. (3) to the temperature dependence of the resistivity of SWCNT-based material (T_0 = 47.83 K).

Fig. 5. Dependence of current fluctuation spectral density: (a) on frequency (when the flowing current is approximately equal to 1 μA); and (b) on current (at 86.13 Hz and 290 K).

Fig. 6. Temperature dependence of current noise spectral density at 86.13 Hz, when the current flowing at room temperature is approximately equal to 1 μA.

Fig. 7. Current noise spectral density versus resistivity at 86.13 Hz when the current flowing at room temperature is approximately equal to 1 μA. The solid lines are the best fits of Eqs. (7) and (8) to the experimental data.

Table 1. Parameters of resistivity and noise temperature characteristics of investigated materials

Filler	$T_{\min R}$, K	T_1, K	T_0, K	$T_{\text{noise max}}$, K
EG	229	80	208	237
CBH	187	547	154	288
SWCNT	292	108	48	276

$T_{\min R}$: temperature of the minimum of resistivity; T_1 and T_0 : parameters of equation (3); $T_{\text{noise max}}$: temperature of the maximum of current noise spectral density.

Fig. 1

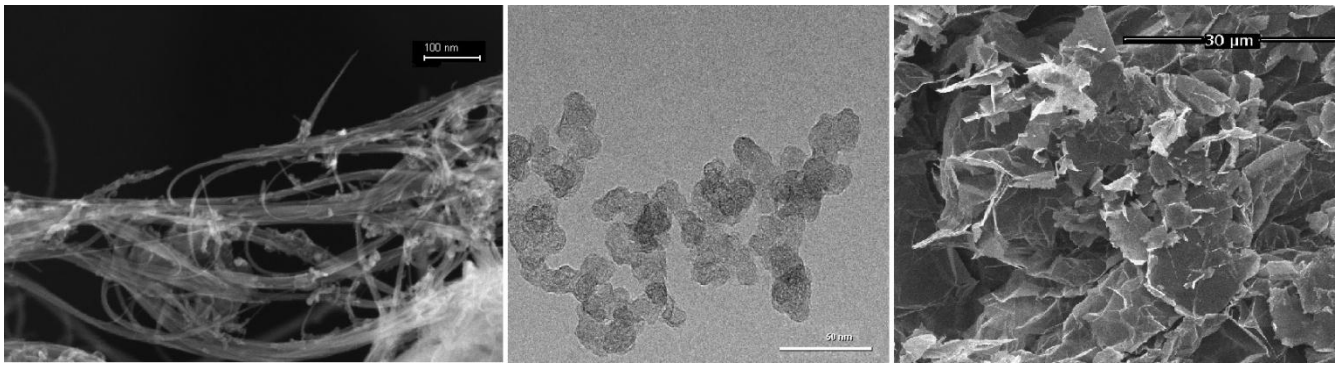

Fig. 2

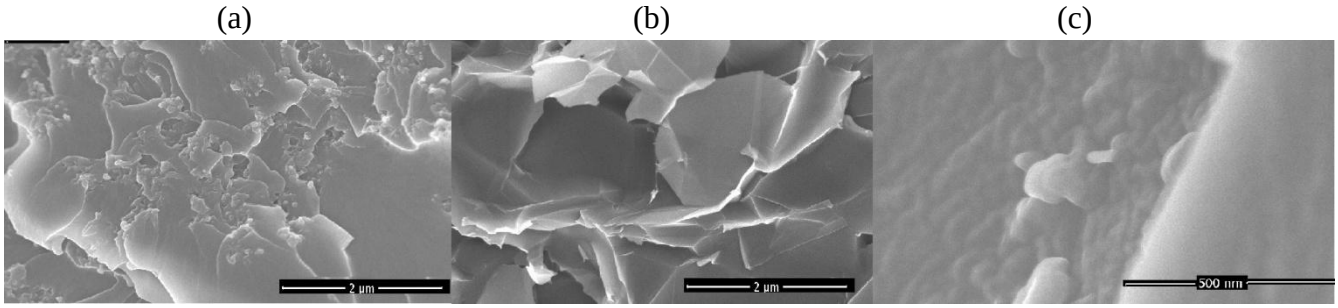

Fig. 3

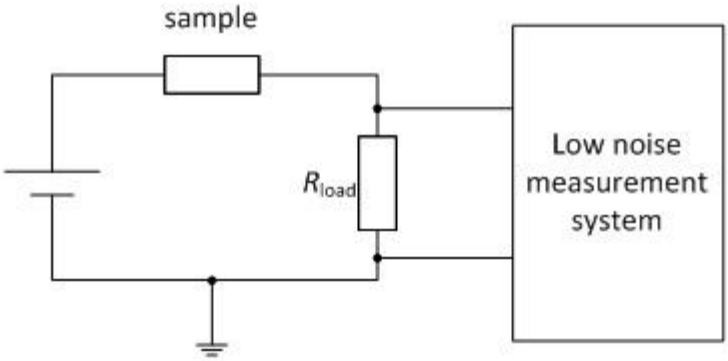

Fig. 4

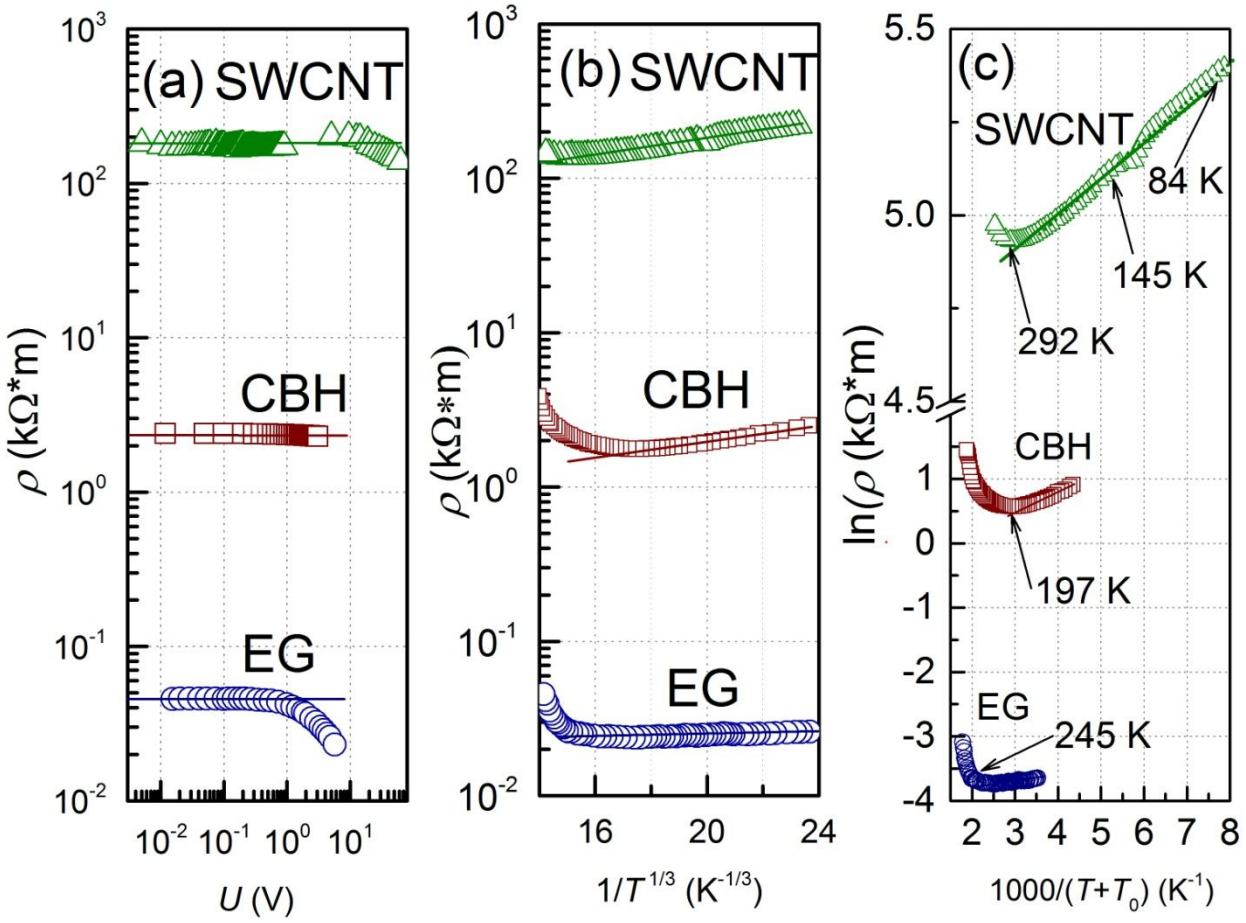
(a) SWCNT
CBH
EG
ρ (kΩ*m)
U (V)
(b) SWCNT
CBH
EG
ρ (kΩ*m)
1/T^1/3 (K^-1/3)
(c)
SWCNT
84 K
145 K
292 K
CBH
197 K
EG
245 K
ln(ρ (kΩ*m)
1000/(T+T0) (K^-1)

Fig. 5

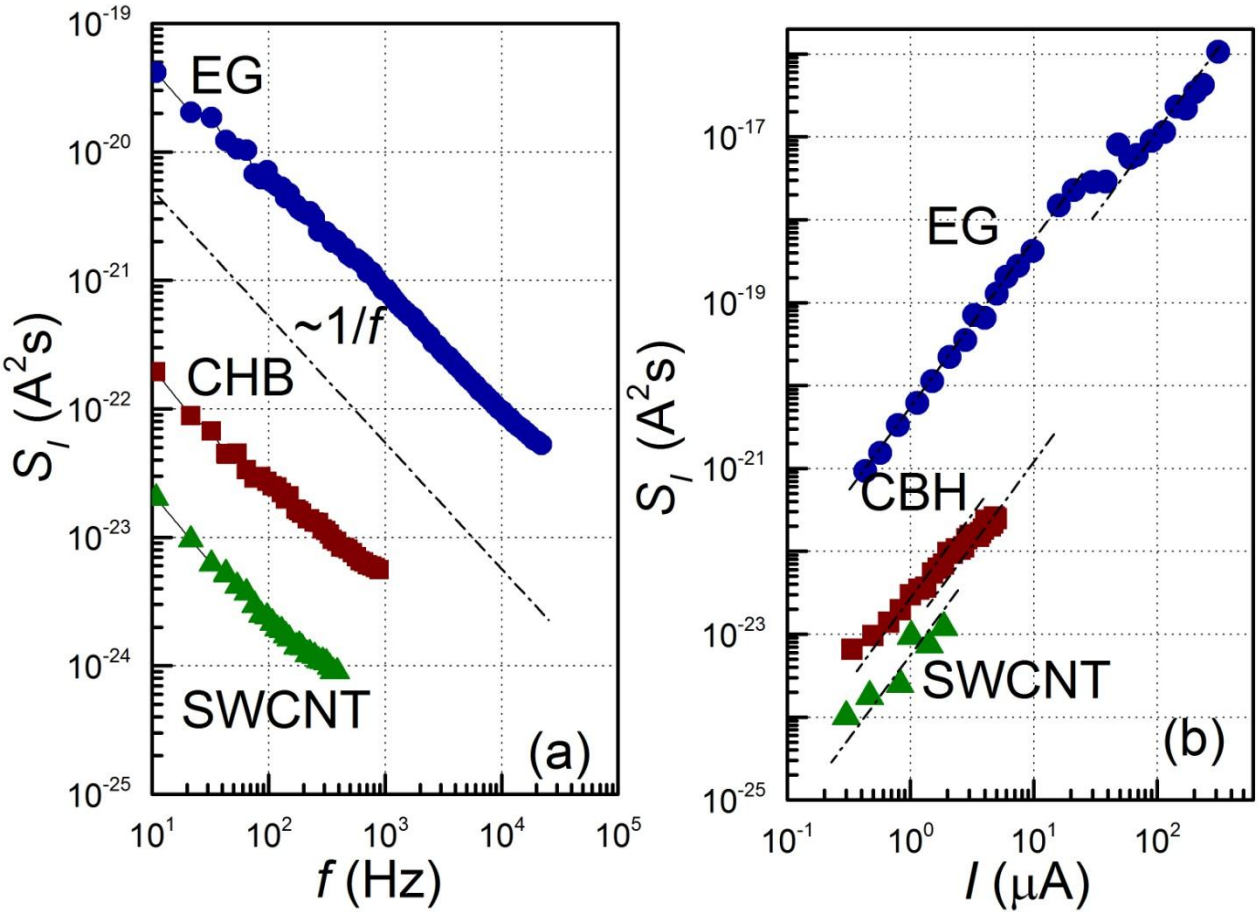
EG
CHB
SWCNT
~1/f
(a)
S_I (A^2s)
f (Hz)
10^{-19}
10^{-20}
10^{-21}
10^{-22}
10^{-23}
10^{-24}
10^{-25}
10^{1}
10^{2}
10^{3}
10^{4}
10^{5}
EG
CBH
SWCNT
(b)
S_I (A^2s)
I (μA)
10^{-17}
10^{-19}
10^{-21}
10^{-23}
10^{-25}
10^{-1}
10^{0}
10^{1}
10^{2}

Fig. 6

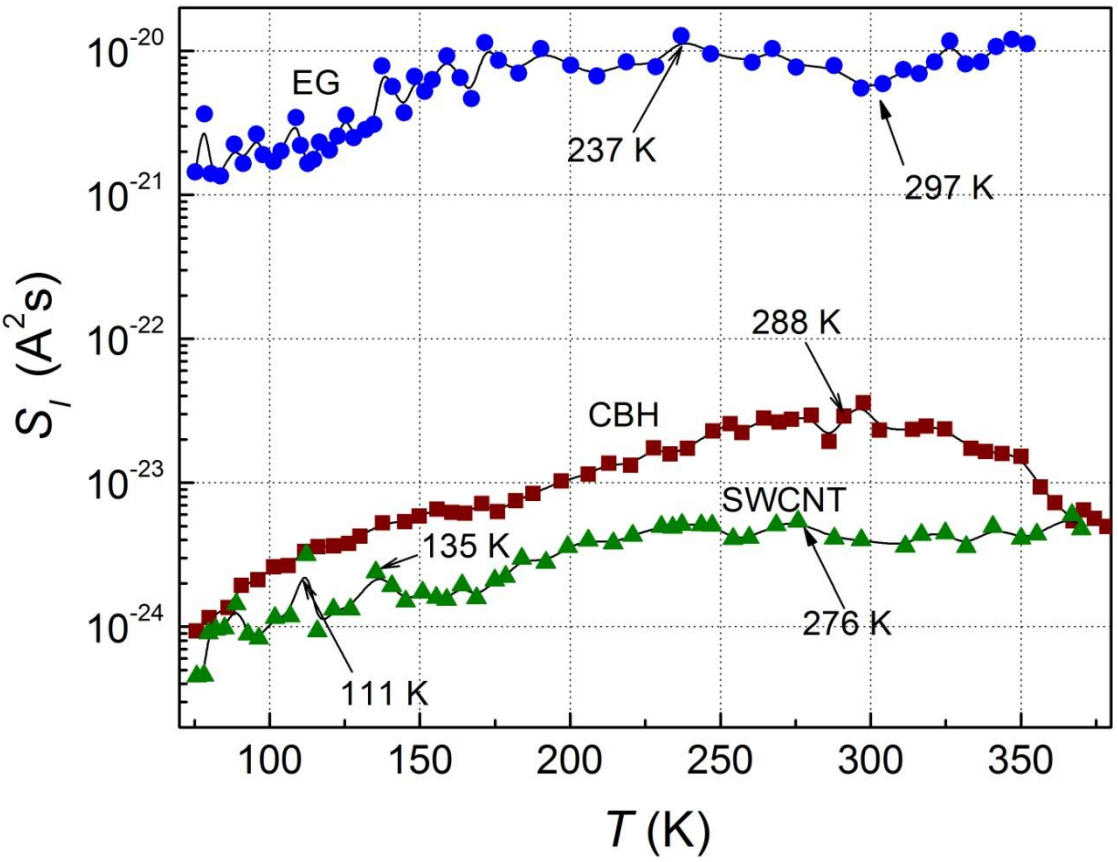
EG
237 K
297 K
288 K
CBH
SWCNT
135 K
276 K
111 K
10^{-20}
10^{-21}
10^{-22}
10^{-23}
10^{-24}
S_I (A^2s)
100
150
200
250
300
350
T (K)

Fig. 7

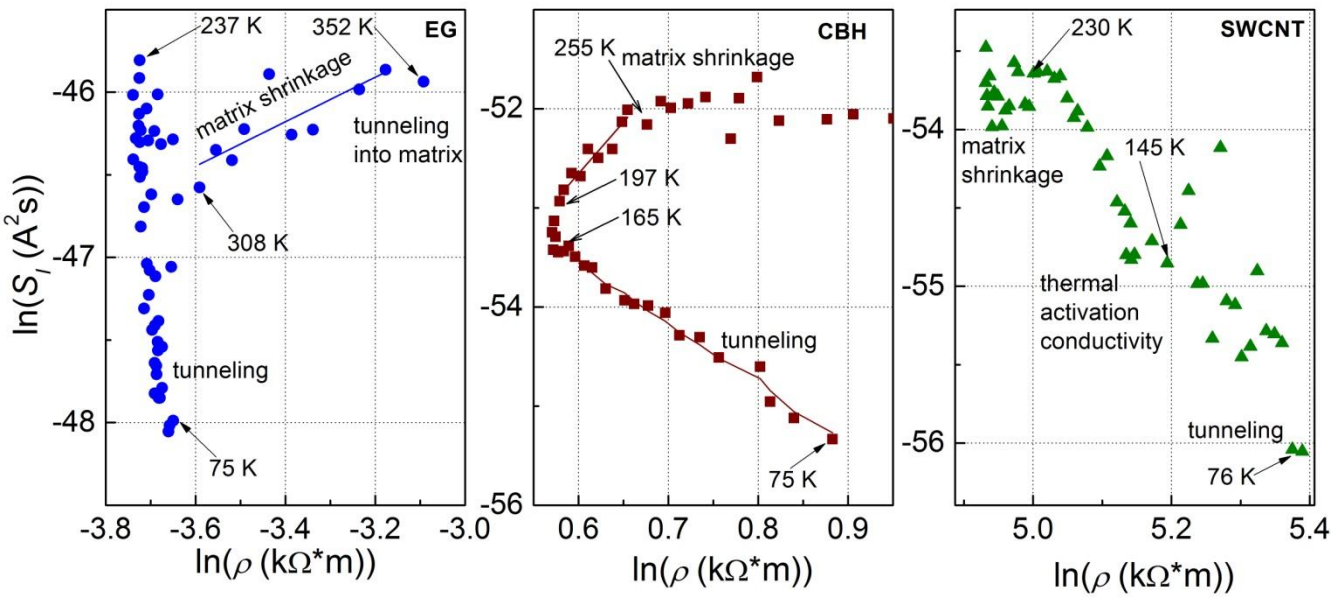
EG
237 K
352 K
matrix shrinkage
tunneling
into matrix
308 K
tunneling
75 K
-46
-47
-48
-3.8
-3.6
-3.4
-3.2
-3.0
ln(S_I (A^2s))
ln(ρ (kΩ*m))
CBH
255 K
matrix shrinkage
197 K
165 K
tunneling
75 K
-52
-54
-56
0.6
0.7
0.8
0.9
ln(ρ (kΩ*m))
SWCNT
230 K
matrix
shrinkage
145 K
thermal
activation
conductivity
tunneling
76 K
-54
-55
-56
5.0
5.2
5.4
ln(ρ (kΩ*m))